Research on Chemical Intermediates
https://doi.org/10.1007/s11164-020-04358-7

Synthesis and characterization of Graphitic Carbon Nitride/ Mesoporous Nano-Silica (g-C_3N_4/KCC-1) nanocomposite as a novel highly efficient and recyclable photocatalyst for degradation of antibiotic in aqueous solution

Marzieh Esmati[1] · Ali Allahresani[2] · Ali Naghizadeh[3]

Received: 3 September 2020 / Accepted: 11 December 2020

Abstract

Among the pharmaceutical compounds, penicillin G (PG) antibiotic has frequently introduced in waters and wastewater. The present study has investigated a novel Graphitic Carbon Nitride/ Mesoporous Nano-Silica (g-C_3N_4/KCC-1) nanocomposite for photocatalytic degradation of PG in aqueous solutions. A facile method applied for catalyst synthesis in different condition, and it was structurally and morphologically characterized using Field Emission Scanning Electron Microscopy (FESEM), Transmission Electron Microscopy (TEM), X-ray Diffraction (XRD), Fourier Transform Infrared Spectroscopy (FTIR), Energy-Dispersive X-ray Spectroscopy (EDAX) and Thermo Gravimetric Analysis (TGA) which showed successful synthesis of g-C_3N_4/KCC-1 nanocomposite. The degradation process was examined as a function of pH (3–11), catalyst dose (0.2–0.8 g/L), contact time (10–120 min) and initial PG concentration (10–100 mg/L) under UV radiation. The results demonstrated that maximum degradation of PG was 93.98% in optimized environmental conditions including pH: 7, nanocomposite dosage: 0.6 g/L, contact time: up to 120 min and initial PG concentration: 10 mg/L. Also, datasets were better explained by Langmuir–Hinshelwood model to defining the kinetic of PG degradation in examined conditions.

✉ Ali Naghizadeh
al.naghizadeh@yahoo.com

[1] Department of Environmental Health Engineering, Student Research Committee, Faculty of Health, Birjand University of Medical Sciences, Birjand, Iran

[2] Department of Chemistry, Faculty of Science, University of Birjand, Birjand, Iran

[3] Medical Toxicology and Drug Abuse Research Center (MTDRC), Birjand University of Medical Sciences, Birjand, Iran

Published online: 05 January 2021

Graphical abstract

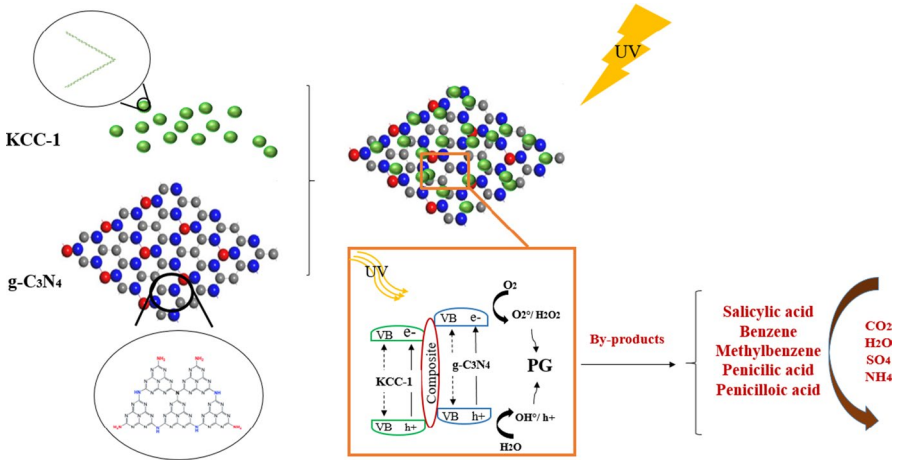

Keywords Antibiotics · g-C_3N_4/ KCC-1 nanocomposite · Photocatalytic · Kinetics · Penicillin G

Introduction

Over the past three decades, the abundant application and stability of pharmaceutical compounds in the environment have made them as the most important pollutants of water [1–3]. Meanwhile, antibiotics are essential antibacterial drugs which applied for prevention of many infectious human and animal diseases [4]. Studies have been show that between 100,000 and 200,000 tons of antibiotics are used in worldwide each year which is increasing now [5,6]. Antibiotics compounds enter the aquatic environment through various sources such as pharmaceutical industries, hospital effluents, and laboratory activities as well as excretion from humans and livestock. Regarding about 30–90% of these compounds are not metabolized in human or animal bodies completely, therefore the residuals and metabolites from antibiotics enter the environment through urine and feces [7,8]. The amount of these compounds in some sources such as hospitals wastewater, municipal effluent and as well as water resources are in the range of µg/L and in other sources such as pharmaceutical industry wastewater is in the range of mg/L [2,9]. Due to the resistance of antibiotics; they are not degraded in conventional wastewater treatment processes and eventually enter to the natural ecosystems [10–14]. Hence, it is expected that these compounds will be found at high amounts in water resources [4]. On the other hand, the presence of antibiotics in the aquatic solution led to expanding antibiotic-resistant genes and bacteria which have adverse effects on human health and other organisms [15]. Penicillin G, due to its low cost and high performance against gram-positive and gram-negative

bacteria, used as a general antibiotic in the world so that only about 20 countries produced 11 thousand tons of this compound every year. Also this antibiotic is solvable in water and is classified as a weak monocarboxylic acid ($pk_a = 2.75$) [16,17]. The reaction mechanisms in this group include cell wall destruction and inhibition of peptidoglycan production in bacteria [18]. According to some of the previous literature, high concentrations of penicillin types reach about 400 mg/L in some wastewater sources [19]. Therefore, the use of effective and efficient methods seems to be necessary for reducing the entry of this antibiotic into the environment.

In order to the degradation and removing the antibiotic substances from aqueous environments, a lot of methods including chemical, physical and biological techniques have been used. From these techniques, adsorption, membrane filtration, ozonation processes, ion exchange, photo-catalysis, and advanced oxidation are more common [15,20–24]. Among mentioned techniques, photocatalytic degradation processes using UV radiation due to cost-effective, high efficiency, and safe production of by-products (CO_2 and H_2O) are known suitable for degradation of PG compared to other treatment processes [25–28]. Also, since these processes use solar renewable energy, expanded as a viable alternative compared to high-energy consumption processes. This method operate through the absorption of photons contains similar energy or greater than the catalytic band gap energy used [29–31]. Following the energy absorption, an electron (e^-) of the catalyst is transferred from the valence band to the conduction band which creates a photo-generated hole (h^+) in the valence band. It oxidizes water molecule to produce hydroxyl radicals (OH°) in aqua that are strong oxidants. Finally, produced OH° radicals can degrade many organic compounds such as PG through their oxidation which is the focus of this present study [32,33].

The catalysts used in this study for photocatalytic degradation are synthesized using different methods with various basic materials.

In recent years, mesoporous nano-silica (KCC-1) that is a kind of SiO_2 particle has been considered as a catalyst because of permanent porosity and high specific surface area caused by the presence of large pores and exclusive fibrous morphology. This compound has not been offered alone for superhydrophobic surfaces before [34–36]. Since KCC-1 has a neutral frame, it must be modified to access active sites and enhance the photocatalytic activity that can be done via coating on elemental and semiconductor structures [37]. Up to now, the numerous supporters have expanded for KCC-1 modification such as Ag, TiO_2, Fe_3O_4/SiO_2 and Al [37–40].

Recently, graphitic carbon nitride (g-C_3N_4) has been proposed as a semiconductor photocatalyst [41–47]. Characteristics of this catalyst including non-toxicity, high thermal and light irradiation stability, metal-free structure, large-scale preparation capability, and simple synthesis through polycondensation of organic compounds as melamine have increased its use [42,48–50]. Here we investigate g-C_3N_4 as a new modifier for KCC-1.

In the present report, the first object was to synthesize and characterize of the novel g-C_3N_4/KCC-1 nanocomposite. Then, the application of this photocatalyst was investigated for degradation of PG using simulated sunlight in the laboratory.

Materials and methods

Reagents

All chemicals and reagents such as cetyltrimethylammonium Bromide (CTAB): ($C_{19}H_{42}BrN$), urea (CH_4N_2O), tetraethyl orthosilicate (TEOS) ($SiC_8H_{20}O_4$), cyclohexane (C_6H_{12}), 1-pentanol ($C_5H_{11}OH$), melamine ($C_3H_6N_6$) and ethanol were purchased from Merck Company (Germany). Penicillin G sodium salt ($C_{16}H_{17}N_2NaO_4S$) (purity ≥ 98%) was obtained from Sigma-Aldrich Company (Germany). Chemical and physical properties of Penicillin G are shown in Table 1. The solutions were prepared daily using distilled water. In addition, the pH values of solution were adjusted using 1 molar solution of HCL and NaOH (Merck, Germany).

Catalyst Fabrication

Synthesis of KCC-1

For synthesis of KCC-1, microwave assisted hydrothermal method was used which requires a short time. In brief, 2 g of CTAB and 2.4 g of urea was dissolved in 100 mL of deionized water and then stirred for 15 min at room temperature (solution A). Next, the mixture of 10 mL of TEOS and 10 mL of cyclohexane was added drop wise to solution A under vigorous stirring for 15 min (solution B). In last step, 1-pentanol (6 mL) was slowly added to solution B. This mixture was continuously stirred for 20 min at room temperature to make sure the solutions was homogenous. Finally, the obtained solution was placed in a Teflon-sealed microwave (MW) reactor for 1 h at 120 °C (800 W). After the reaction, the mixture was cooled at room temperature and was separated via centrifugation, then the separated silica was washed with distilled water and ethanol and oven-dried at 120 °C for 8 h and finally calcined at 550 °C for 5 h [51,52].

Synthesis of g-C_3N_4/KCC-1

g-C_3N_4/KCC-1 nanocomposites were prepared by mixing melamine with KCC-1 synthesized according to the following procedure (Fig. 1). To find the best ratio of melamine and KCC-1, several rounds of this nanoparticles were synthesized. For this purpose, different masses of melamine (0.3, 1, 2, 2.5, 3, 3.5, 4 and 4.5 g) dissolved in 3 mL of ethanol solution and were ultrasonically dispersed, then 0.15 g of KCC-1 synthesized added to it. Furthermore, 100 mL of water is added to the previous mixture and stirred for 24 h. The suspension was heated to evaporate the liquid. Eventually, white powder immediately was transferred into an alumina crucible with a cover and calcined in muffle furnace at 550 °C for 4 h under the air at the rate of 2 °C per minute [22]. The ultimate yellow powder

Table 1 Chemical and physical properties of PG

Molecule	Formula	Molecular weight (g/mol)	Solubility (mg/mL)	Density (g/cm^3)	Storage temperature (°C)	Buliding Point (°C)
PG	$C_{16}H_{17}N_2NaO_4S$	356.37	100	1.41	2–8	209–212

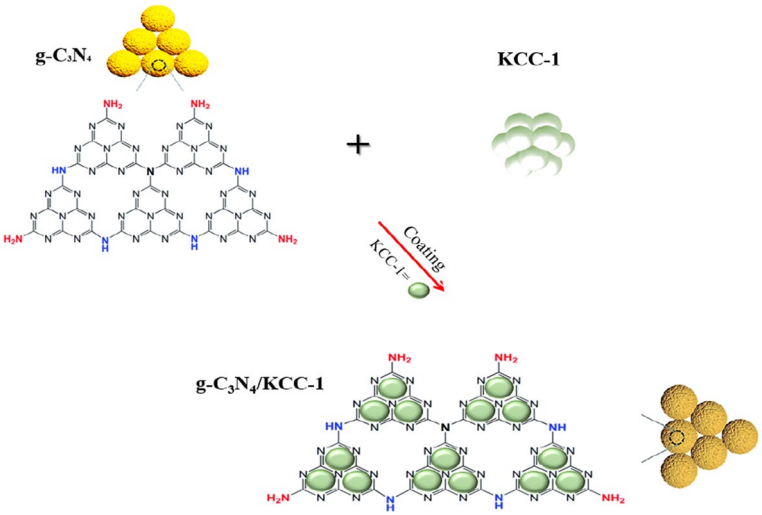

Fig. 1 Schematic representation for the synthesis of g-C_3N_4/KCC-1 nanocomposites

was used for further experiments. All of g-C_3N_4/KCC-1 catalysts were prepared by a similar method.

Characterization of the catalyst

For determination of the surface morphology and characterization of the synthesized g-C_3N_4/KCC-1 nanocomposite, several advanced techniques were used. Field Emission Scanning Electron Microscope (FESEM) (Tescan Mira3 FESEM, Czech Republic) was used for determination of morphology and microstructure of the prepared samples. The morphological specifications, microstructure and average diameter of nanoparticles were specified by Transmission Electron Microscopy (TEM) (Philips, CM120, Holland). X-ray Diffraction (XRD) (Philips, PW1730, Holland) device with Cu K_α radiation ($K = 1.5406$ A$^\circ$) was applied for detection of the changes in the crystalline structure of photocatalyst particles. In order to determination of the functional group type and qualitative identification, Fourier Transform Infrared Spectroscopy (FTIR) (JASCO, FT/IR-4600, Japan) was used at 4000 to 400 cm^{-1} wave number range. Energy-Dispersive X-ray Spectroscopy (EDAX) (Oxford Instruments, United Kingdom) analysis that applied for characterization of elemental distribution was utilized. To determine the amount of organic matter supported on nanoparticles and thermal stability, Thermo Gravimetric Analysis (TGA) was used (Q600, TA Instrument, America). Also, the concentration of Penicillin G was determined by UV/Vis spectrophotometer (T80 + , PG Instrument Ltd, England).

Measurements of pH_{zpc} for g-C_3N_4/KCC-1

The point of zero charge (pH_{ZPC}) defined as the pH where the real charge on the nanoparticles surface is zero. In other to obtain the pH_{ZPC} of g-C_3N_4/KCC-1 nanocomposite, 5 Erlenmeyer which filled with 100 mL of distilled water were applied. Afterward, the initial pH of containers was adjusted in 3, 5, 7, 9 and 11 by the addition of HCl or NaOH solutions. Then, 0.2 g of the synthesized nanocomposite was added to prepared solutions and then were shaken at 250 rpm for 48 h. The pH was read again and recorded as the final value.

Experimental procedure

In this study, the photocatalytic batch reactor was used with a capacity of 500 mL which composed of two separate parts. The internal enclosure was contained 300 mL of the sample in which all reactions occurred here. Another part of this pilot which placed around the main enclosure, used to decrease solution temperature caused by ultraviolet (UV) radiation via applying water circulation. Meanwhile, the UV lamp (Philips, Poland) with wavelength = 253.7 nm, power = 18 W, Life time = 8000 h and irradiation of intensity = 294–282 w/m^2 was installed in the center of the reactor as UV–C irradiation source which surrounded by a quartz jacket. Sampling was carried out via a valve placed at the bottom of the reactor. The schematic of the photocatalytic pilot was shown in Fig. 2. All the experiments were operated at stable conditions in dark situations and 300 rotations per minute at temperature of 23 ± 2. The experiments were performed under the varying ranges of pH solution (3, 5, 7, 9 and 11), reaction time (10, 30, 60, 90 and 120 min), initial PG concentration (10, 30, 50, 70 and 100 ppm) and dose of g-C_3N_4/KCC-1 nanocomposite (0.2, 0.4, 0.6 and 0.8 g/L). For this purpose, the stock

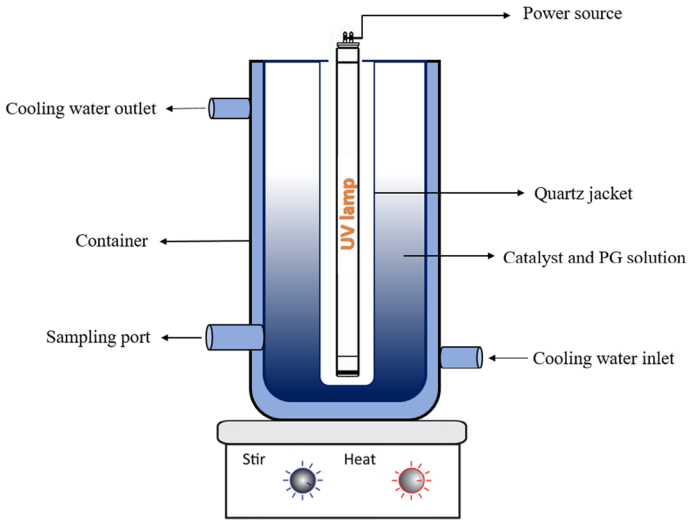

Fig. 2 Schematic of the reactor used in this study

solution of PG was prepared and in order to prevent the effects of other light, all solutions were kept in the dark conditions. The pH of samples that set by HCl and NaOH is determined using pH meter (pH meter Hach, HQ411d, USA). In order to develop the photocatalytic process, the aqueous solution containing g-C_3N_4/KCC-1 nanocomposite placed in an ultrasound bath (Elmasonic, E30H, Germany) for 30 min to disperse the nanoparticles. The compound of PG and nanoparticles was stirred under dark conditions for 30 min and then the UV lamp was turned on. At mentioned time interval of irradiation, 3 mL of samples was taken and centrifuged for 10 min at 6000 rpm (Centurion Scientific, K280R, England). The separated aqueous solutions were measured through spectrophotometer in wavelength of maximal absorption 290 nm. To enhance the separation performance, 0.2-micron filter cartridge and also centrifuge of the samples were used. Since similar results were obtained, the centrifuge method was used for separation of the nanocomposites. Ultimately, degradation efficiency (DE %) was calculated by the following equation. Which C_0 and C_e were initial and residual concentrations of PG, respectively (53):

$$DE\% = \frac{Co - Ce}{Co} \times 100 \tag{1}$$

Kinetic study

In the photocatalytic processes, it could be useful to investigate and evaluate the kinetic degradation parameters for different organic pollutants, especially antibiotics. In this context, the evolution curves that achieved from reaction time at various initial PG concentrations in the photocatalytic process eventually were applied for kinetic modeling. These reactions were defined via the pseudo-first-order kinetic model and applied to the exact design of the wastewater treatment system. In several recent research, the Langmuir–Hinshelwood (L–H) widely used for modeling of the organic materials degradation which can be written as the following Eq. [44,54,55]:

$$r = Kr\theta = -\frac{dc}{dt}Kr\left(\frac{KCo}{1 + KCo}\right) \tag{2}$$

where *"r"* is the reaction rate (mg/L.min), k_r is the constant of reaction rate (1/min), k is adsorption factor, θ is the fractional sites of nanoparticle covered by PG, and C is the concentration of PG at each time. In cases where the pollution concentrations are very low and in poor adsorption or/ and substrate ($KC \ll 1$), such like drugs in water, Equation can be made simple as follows:

$$-\frac{dc}{dt}KrKC = Kot \tag{3}$$

$$\ln\left(\frac{C}{Co}\right) = -Kot \tag{4}$$

where *"t"* is reaction time, C_0 and C_t are the initial and residual concentration of PG, respectively, k_0 is the rate constant of the pseudo-first-order. In addition, the coefficient of regression (R^2) utilized for determination of the fit accuracy between kinetic models and testing results.

Results and discussion

In this study, synthesis of g-C_3N_4/KCC-1 nanocomposite was carried out for reaching the optimum photocatalytic function. Fig. 3 summarizes degradation efficiency for several modification strategies based on changes in melamine content with optimizing the condition of experiments. According to the results, the degradation of penicillin G increases with an increasing amount of melamine in the synthesized catalyst, which is highest in high values as specified in Fig. 3. So, all photocatalytic experiments and characterization studies in this research were reported for synthesized nanoparticles containing 2 g of melamine and 0.15 g of KCC-1 catalyst. Meanwhile, Hydrogen peroxide was also used to improve the efficiency of photocatalytic experiments but was less effective in the degradation of penicillin.

Characterization study

FT-IR analysis

To demonstrate the chemical structure and functional groups of g-C_3N_4/KCC-1 nanocomposite and KCC-1 samples, the FT-IR spectra were employed in the range of 4000–400 cm^{-1}. According to Fig. 4, the spectra of g-C_3N_4/KCC-1 synthesized under similar conditions with different amount of melamine (0.3, 1, 2, 2.5, 3, 3.5, 4 and 4.5 g) were nearly similar, except for spectrums which contained

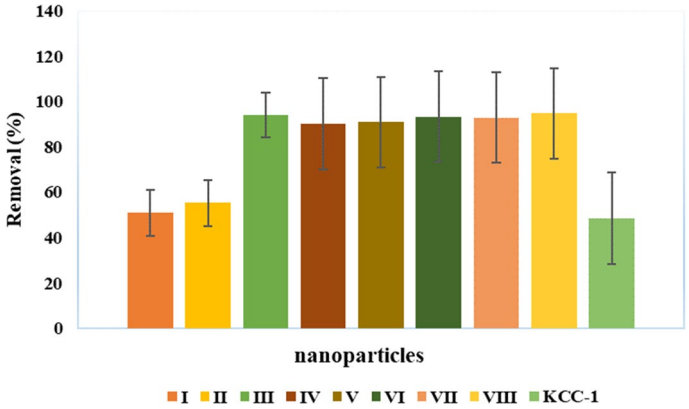

Fig. 3 Influence of various nanocomposite synthesized on photo-degradation processes: I (g-C_3N_4/KCC-1 (0.3 g + 0.15 g)), II (g-C_3N_4/KCC-1 (1 g + 0.15 g)), III (g-C_3N_4/KCC-1 (2 g + 0.15 g)), IV (g-C_3N_4/KCC-1 (2.5 g + 0.15 g)), V (g-C_3N_4/KCC-1 (3 g + 0.15 g)), VI (g-C_3N_4/KCC-1 (3.5 g + 0.15 g)), VII (g-C_3N_4/KCC-1 (4 g + 0.15 g)), VIII (g-C_3N_4/KCC-1 (4.5 g + 0.15 g)) and KCC-1

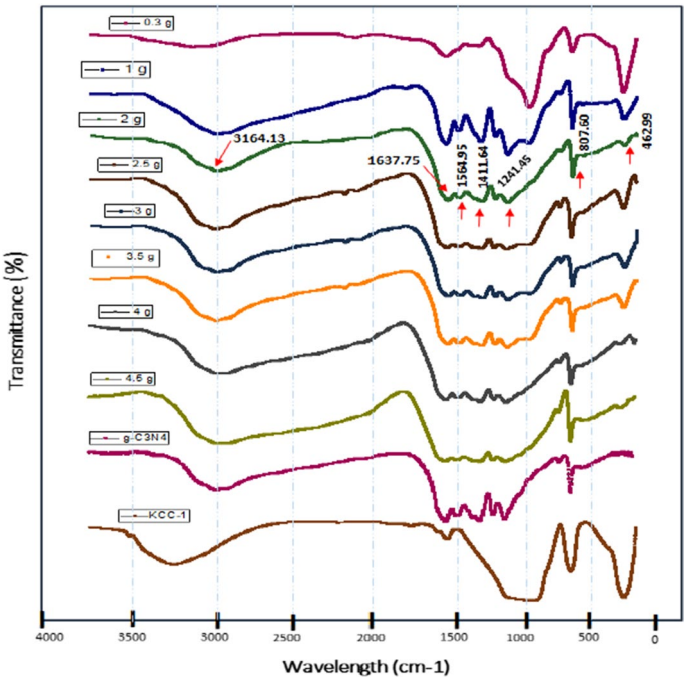

Fig. 4 FTIR spectrum of g-C_3N_4/KCC-1 (0.3 g + 0.15 g), g-C_3N_4/KCC-1 (1 g + 0.15 g), g-C_3N_4/KCC-1 (2 g + 0.15 g), g-C_3N_4/KCC-1 (2.5 g + 0.15 g), g-C_3N_4/KCC-1 (3 g + 0.15 g), g-C_3N_4/KCC-1 (3.5 g + 0.15 g), g-C_3N_4/KCC-1 (4 g + 0.15 g), g-C_3N_4/KCC-1 (4.5 g + 0.15 g), g-C_3N_4 and KCC-1

from dosage 0.3 and 1 g of melamine along with 0.15 g of KCC-1. This indicates the mentioned samples are not properly synthesized and the result in Fig. 3 can reflect it. Other spectra assigned to the incorporated mesoporous nano-silica in graphitic carbon nitride are represented the accurate synthesis. For g-C_3N_4/KCC-1 nanocomposite, the broad peaks between 3000 and 3500 cm^{-1} wave number were corresponding to the free amino groups (N–H) and hydroxyl types (O–H) that can be attributed to stretching vibration mods [56]. In addition, the sharp band located near 808 cm^{-1} is due to specific breathing of s-triazine rings [57]. The powerful bands detected at 1200 to 1700 cm^{-1} region are shown as C-N groups which the two absorption peaks observed at 1500–1700 cm^{-1} were related to the tensile vibrations, while the bands were found in the range of 1200–1500 cm^{-1} are assigned to stretching vibration in CN heterocycles. The adsorption peak at 1637 cm^{-1} is shown fine crystallization of synthesized g-C_3N_4 [58–60]. Moreover, the three major bands found in the FT-IR spectra of pure mesoporous KCC-1 at 1095, 802 and 464 cm^{-1} were ascribed to the vibrational mode of Si–O-Si functional groups. Besides, the OH band related to stretching vibrations of Si–OH is responsible for the peak which appeared in 3000–3600 cm^{-1} [61].

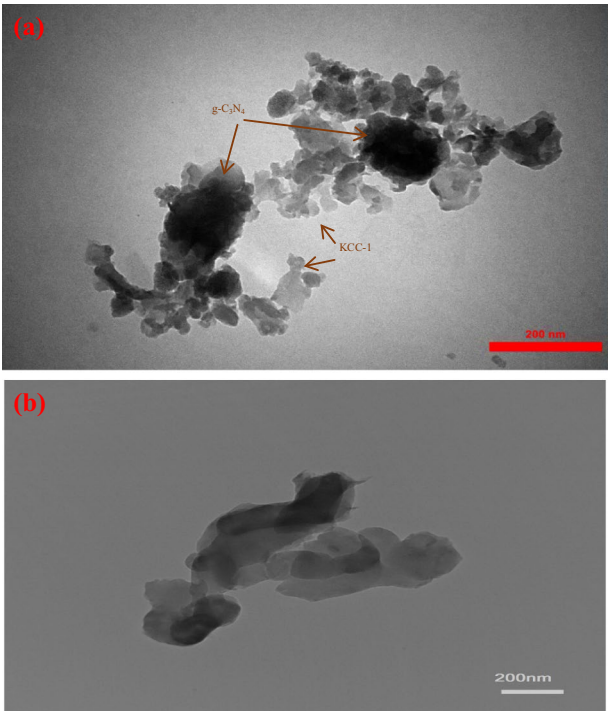

Fig. 5 TEM image of a synthesized **a** g-C_3N_4/KCC-1 nanocomposite and **b** g-C_3N_4 nanosheets

TEM analysis

The microstructure and morphology of graphitic carbon nitride-supported silica nano-catalyst and graphitic carbon nitride nanoparticle confirmed through TEM are illustrated in Fig. 5. In the heterojunction samples, the darker part should be the g-C_3N_4 which displayed as large bulk with a sheet-like structure at the diverse diameters [62–64]. Based on published studies, KCC-1 generally has a fibrous morphology [34]. The lighter particles with gray colored areas can be KCC-1 marked nonuniform in figure. It is apparent that numerous KCC-1 nanoparticles with a diameter in nanometers scale are anchored on the g-C_3N_4 nanosheets surface in the synthesized catalysts morphology and aggregation was nearly specified. This coating is desirable for the charge transfer between g-C_3N_4 and KCC-1 catalysts (65). Also, interestingly, the average size of the particle was about nanometers scale.

FESEM analysis

The FESEM of the g-C_3N_4/KCC-1 further verifies the microstructure of nanocomposites. Fig. 6 depicts the FESEM image for the synthesized samples. As evident from the micrograph, the disorderly stacked and sheet-like accumulation of g-C_3N_4

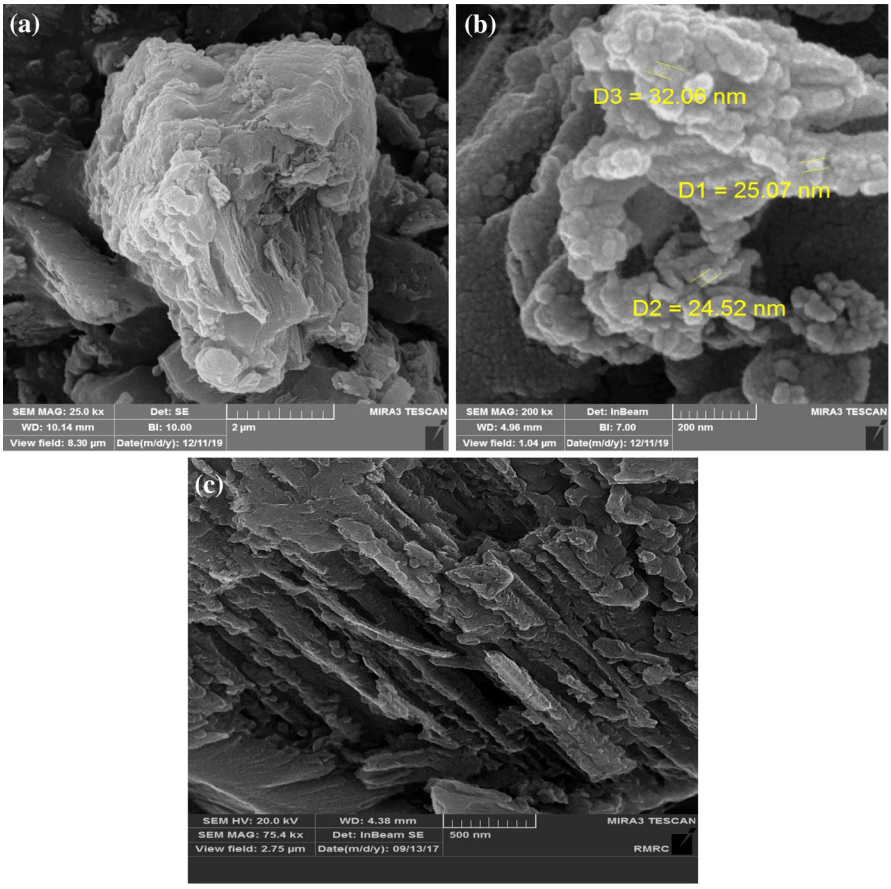

Fig. 6 FE-SEM image of **a** and **b** synthesized g-C_3N_4/KCC-1 nanocomposite and **c** g-C_3N_4 nanosheets

is clearly observed in the g-C_3N_4/ KCC-1 nanocomposite (Fig. 6a and c). While in higher resolution, the KCC-1 nanoparticles seem to be less than 40 nm which are partially aggregated and accumulated after attached on the g-C_3N_4 and it forms the homogenous (Fig. 6b).

XRD analysis

Figure 7 shows the XRD patterns of original and final synthesized g-C_3N_4/KCC-1 nanocomposite to investigate the structure of KCC-1 after modifying with g-C_3N_4. These patterns provide information about the crystallographic structures and proximate size of nanoparticles [66]. As seen in this figure, two specific peaks around 27.5° and 13.4° are related to the g-C_3N_4 crystalline structure which indexed to (0 0 2) and (1 0 0) planes and can be classified for graphitic substances. The strong and sharp peak at 27.5° is due to interplanar stacking of aromatic rings and

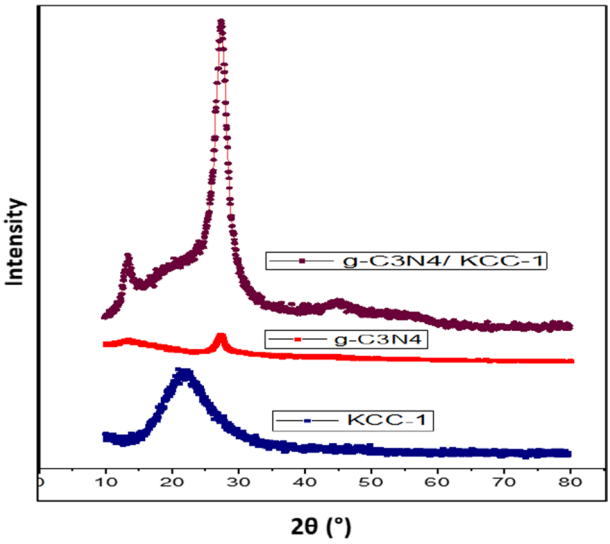

Fig. 7 XRD patterns of g-C_3N_4/KCC-1 nano-composite, g-C_3N_4 and KCC-1

the small-angle peak presented at 13.4° is relevant to the in-plane structural packing motif. Meanwhile, two recorded diffraction peaks are an agreement with the other reported results [22,55,67]. According to studies, the XRD spectra of KCC-1 confirm a wide-angle peak in 20° to 25° range. Since the position and shape of the g-C_3N_4/KCC-1 peak have not changed, it can be stated that the structure of the g-C_3N_4 nano-layer does not change with KCC-1 modification and the supported incorporated into the lattice of g-C_3N_4 [35,43,68].

The Debye–Scherrer equation was used to approximate the crystallite size via the maximum peak through the following:

$$D = \frac{K\lambda}{\beta \cos\theta} \tag{6}$$

where D is the diameter of nanoparticles, k is dimensionless shape factor that has a typical value of about 0.9, λ is the X-ray wavelength equal to 1.54 Å, θ is the Bragg angle and β is full-width at half the maximum intensity (FWHM).

The results of the calculations indicated that the crystallite size of the g-C_3N_4/KCC-1 nanocomposite was about 8 nm.

TGA analysis

The TGA analyses define the material mass changes, volatile content and thermostability according to temperature and time processes [69]. In this study, the thermal properties of g-C_3N_4/KCC-1 nanocomposite investigated under the air atmosphere from ambient temperature to 800 °C at a heating rate of 10 °C min^{-1}. As can be seen in Fig. 8, it is evident that from a temperature of 28 to 500 °C insignificant weight

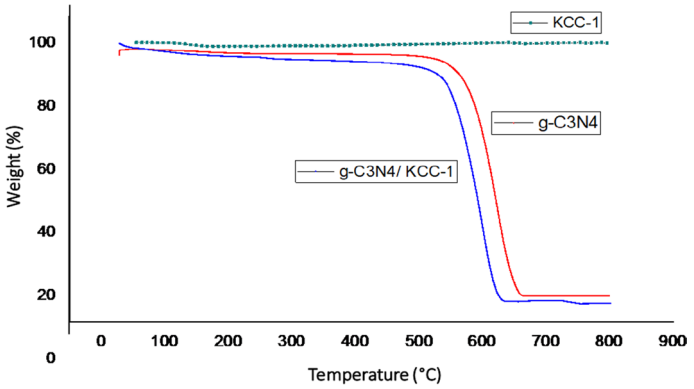

Fig. 8 Thermogravimetric analysis of g-C_3N_4/KCC-1 nano-composite, g-C_3N_4 and KCC-1

change is depicted in the TGA curve of the nanocomposite. Decomposition of g-C_3N_4/KCC-1 starts at 550 °C with the rapid decay of TGA curve and is completed at 630 °C. This could be due to the chemical conversion of g-C_3N_4 to carbon and nitrogen containing gases and also the loss of hydroxyl groups from KCC-1 [70–72]. Eventually, a weight loss of 98.53% was observed in the range of temperature range analysis which the maximum was above at 550 °C and after about 630 °C fixed.

EDAX analysis

EDAX spectra were used for demonstration of the elemental composition of g-C_3N_4/KCC-1. Fig. 9 shows peaks corresponding to elements making up the composition of the sample being analyzed. According to results, the percentage of C, N, O, and

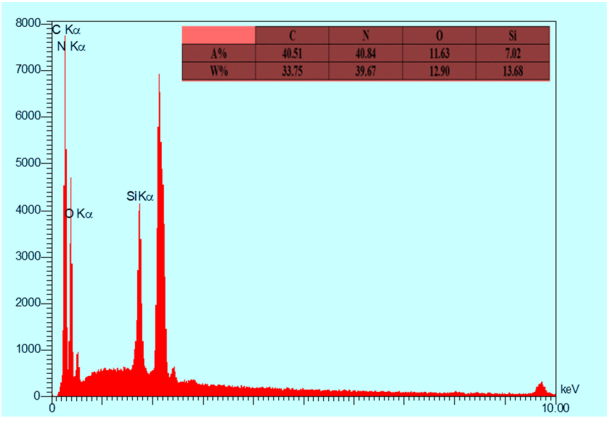

Fig. 9 EDAX spectrum of g-C_3N_4/KCC-1 sample

Si were 40.51, 40.84, 11.63 and 7.02, respectively. The EDAX of nanocomposite confirms the presence of the above elements in the desired W%.

Optical properties determination

Figure 10 shows UV–vis diffuse reflectance spectra that revealed the absorption spectrum of the catalyst between 200 and 800 nm. According to studies, KCC-1 is possess an absorption in the area less 280 nm and characteristic absorption wavelength of g-C3N4 onset at about 450 nm. As predicted the absorption g-C3N4/KCC-1 nanocomposite occurs at wavelengths region shorter than 400 nm and it highest in 295 nm (73–77).

Experiments of catalyst

Measurement of pH_{pzc}

For these objective, according to the method described above, 5 Erlenmeyer flasks were filled with 100 ml of water containing g-C_3N_4/KCC-1 nanocomposite in various pH. After a specified time stirred at room temperature, the final pH was measured and compared to the initial pH. pH_{pzc} is the isoelectric point where the graph of initial pH cross from ultimate pH and as the results show, the absorber isoelectric point is about 6.8 value (Fig. 11).

Influence of pH

In the photocatalytic process, the solution pH is an effective factor in degradation and adsorption capacity of organic compounds since it defines the surface charge and size of the nanocatalyst aggregates [78]. This parameter has a significant effect

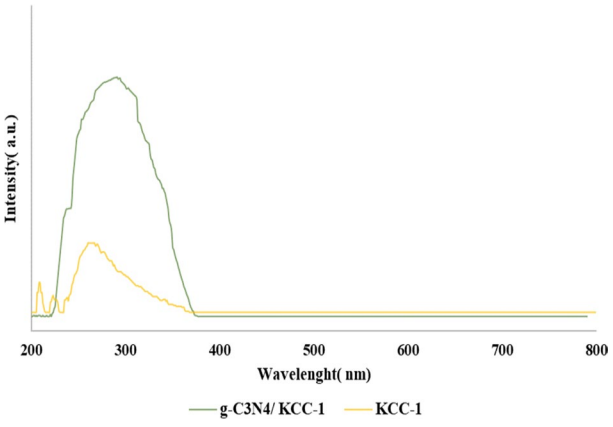

Fig. 10 UV–vis diffuse reflectance spectra (DRS) of KCC-1 and g-C_3N_4/KCC-1 nanocomposite

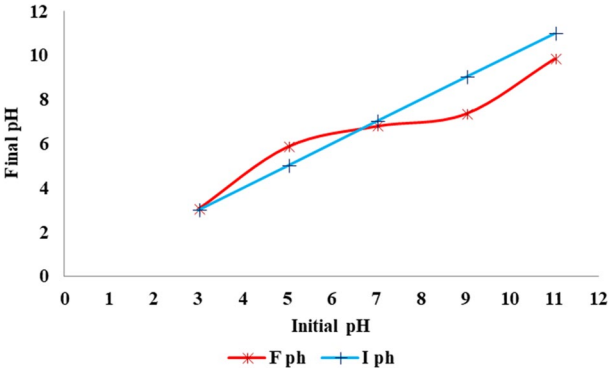

Fig. 11 Zeta potential of g-C_3N_4/KCC-1 nanocomposite

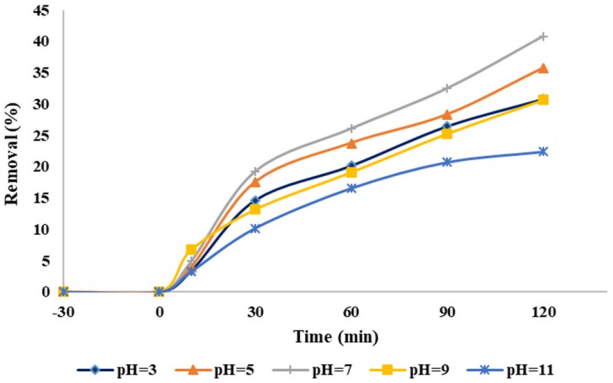

Fig. 12 Effect of pH in photocatalytic degradation of PG by g-C_3N_4/KCC-1 nanocomposite (PG concentration: 30 mg/L, catalyst dosage: 0.2 g/L)

on dissolution property of antibiotics, reaction kinetics, generation of radicals hydroxyl and surface charge characteristics of catalyst [79,80]. Fig. 12 shows the effect of pH changes on PG photocatalytic degradation in the presence of g-C_3N_4/KCC-1 nanocomposite. In other to evaluate the influence of initial pH, the experiments were conducted by different pH [3–11] and fixing the other operating conditions (initial PG concentration = 30 mg/L, photocatalyst dosage = 0.2 g/L and reaction time = 120). The results highlighted which the performance of photocatalytic process was low in the alkaline pH and maximum efficiency achieved by decreasing pH in 7 value. This property has made g-C_3N_4/KCC-1 a desirable and eco-friendly nanoparticle in degradation of PG because approximately all of the water and wastewater are generally in neutral range of pH. However, efficient photodegradation of PG was observed at whole pH values. Meanwhile, as mentioned, the effect of pH parameter on PG degradation can be explained by the charge distributions on the utilized catalyst surface and the antibiotic molecules dissolution. As is well known, the solubility of PG in water specified via the acid dissociation constant (pK_a) that

has been measured 2.75. Therefore, PG molecules predominantly tend to become anionic at pH above pK_a and below of pK_a value have a neutral state [81,82]. In addition, the nanoparticles surface charge surveyed with determining the pH_{zpc} analysis which based on previous founds in this study was equal to about 6.8 (Fig. 11). Thus, the surface of the prepared photocatalyst in higher values than 6.8 will be saturated by negative charges of hydroceles ions and at lower than pH_{pzc} has a positive charge caused by H^+ protons. As a conclusion, the electrostatic repulsive force between PG anionic form and the negative surface load of nanoparticles in pH above neutral causes to decrease percentage of PG degradation. On the other hand, two predominant factors that can play a major role in antibiotic degradation are photo-induced holes in medium acidic conditions and generation of radical hydroxyl in alkaline or neutral solution. Hence, the positive holes (h^+) with top oxidation potential act as producer of hydroxyl radical on g-C_3N_4/KCC-1 surface from water molecules, while insoluble compounds formation and decompose of hydroxyl radical may be the reason for the low degradation of PG in high pH as shown in Fig. 12 [61,81]. The results are consistent with photocatalytic degradation report of organic compounds using TiO_2 particles [83].

Influence of catalyst dosage

Economically, the optimization of catalyst dosage seems necessary before applying in the photocatalytic treatment process. For this objective, the effect of g-C_3N_4/KCC-1 dosage on PG photolysis was examined within the several ranges from 0.2 to 0.8 g/L in pH = 7, reaction time up to 120 min and PG concentration = 30 mg/L. The results showed that the degradation rate increased from 40.79 to 55.1 percentage for 0.2 and 0.6 g/L, respectively, and then decreased again (Fig. 13). Therefore, the highest degradation was observed at a dose of 0.6 g/L. Also, the results showed the concurrent influence of the increasing nanocatalyst dosage and reaction time. This phenomenon can be explained via active sites on the catalyst surface and decrease in intensity of UV light received in solution [81]. In fact, increasing the catalyst dosage

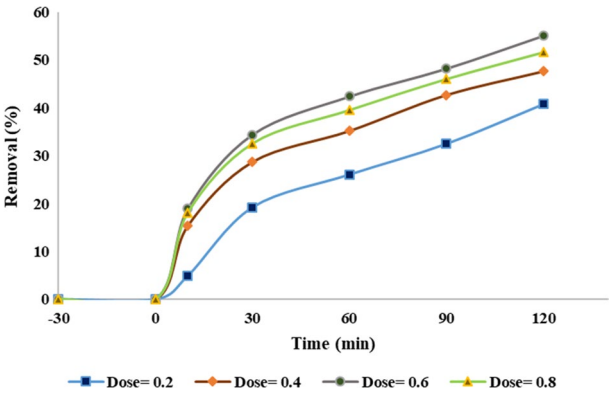

Fig. 13 Effect of g-C_3N_4/KCC-1 dose on the PG removal efficiency (pH = 7, initial PG concentration = 30 mg/L)

has led to create turbidity and eventually decrease the light transmission through the solution. Meanwhile, the occurrence of the agglomeration in nanoparticles at higher than 0.6 g per 1 L solution is another reason for reducing in PG degradation [8,84]. It suggests that the contaminant access to active sites on the nanocatalyst surface and production of hydroxyl radicals improve the process by raising the amount of catalyst in the reactor. The function of catalyst loading under the various conditions in the photocatalytic process surveyed by many researchers. For instance, degradation of β-lactam antibiotics by ZnS nanoparticles and also photocatalytic degradation of azithromycin using GO@Fe_3O_4/ZnO/SnO_2 nanocomposites reported similar results with the present study [19,85].

Generally, increasing the catalyst dose produces more free electrons that react with dissolved oxygen in solution and water molecules, which are responsible for generate highly reactive $OH^{\cdot}$ and $O_2^{-\cdot}$. These radicals are important as facilitators of the photocatalytic activity and PG molecules oxidized. Furthermore, the surface of the catalyst outer shell in the presence of high rate UV light excited and comprised more fine pores that increase the reaction sites of utilized catalyst and as a result improve degradation rate of organic molecules.

On the basis of the mentioned results, the mechanism of PG degradation in the presence of g-C_3N_4/KCC-1 nanocomposite and under UV light was proposed in Eqs. 7–12.

$$h\nu + \text{Photocatalytic reaction} \rightarrow h^+ + e^- \tag{7}$$

$$H_2O + h^+ \rightarrow OH^{\bullet} + H^+ \tag{8}$$

$$OH^- + h^+ \rightarrow OH^{\bullet} \tag{9}$$

$$O_2 + e^0 \rightarrow O_2^{\bullet -} \tag{10}$$

$$O_2^{\bullet -} + H^+ \rightarrow HO^{\bullet} \tag{11}$$

$$HO^{\bullet}/H^+/O_2^{\bullet -} + PG \rightarrow \text{Products} \tag{12}$$

Influence of contact time and PG concentrations

The mechanism of PG decomposition was further evaluated in the initial concentration range of 10–100 mg/L at the varied reaction time (10–120 min) under optimum conditions. Based on Fig. 14, the degradation rate was the highest in the primary stages and decreased from 93.98 to 13.82% with an increase in the PG concentration from 10 to 100 mg/L at reaction time of 120 min. The first reason may be the high prepared concentration of PG antibiotics decreased the available active sites in catalyst surface through the junction of more pollutant molecules. Secondly, the OH° radicals produced were not enough since these agents were constant as the

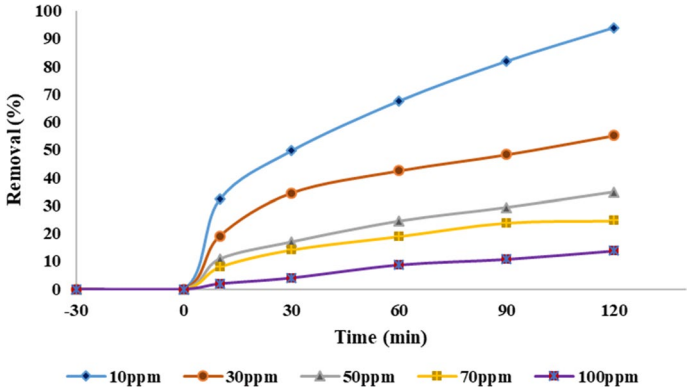

Fig. 14 Effect of PG concentration and contact time on its degradation process by g-C_3N_4/KCC-1 nanocomposite (pH: 7, catalyst dosage: 0.6 g/L)

nanocatalyst dose was equal in all of the prepared solutions, and thereby, leads to an inhibitive influence in PG photolysis. The third explanation can be the photons received by the photocatalyst surface decrease in high amounts of antibiotic because the UV light is absorbed by PG molecules and intermediate products.

According to results, the photo-degradation rate enhanced along with the photocatalytic time. Moreover, at the initial 60 min of photocatalytic reaction time, the PG degradation rate was highest. These can be further explained as the contact time increases, production of the positive holes and also the number of OH° radicals have increased similarly and the process is more effective in early times. Actually, rapid degradation behavior by g-C_3N_4/KCC-1 nanocomposite in early times provides a suitable condition for large-scale use in wastewater containing PG contaminants. As a final conclusion it can be stated that the maximum degradation was achieved 93.98% at 120 min contact time and PG concentration of 10 mg/L.

Kinetic study of PG degradation

The behavior of kinetic for PG degradation in various ranging concentration from 10 to 100 ppm and optimum state (nanocomposite dosage = 0.6 g/L, pH = 7) using the Langmuir–Hinshelwood model is shown in (Fig. 15). The calculation parameters of liner L–H model reaction rate (k_0) which obtained from the plot gradient of $\ln\left(\frac{Co}{Ct}\right)$ versus irradiation time is listed in (Table 2). Based on the data, a notable decrease in (k_0) values with increasing PG initial concentration was indicating a high rate of g-C_3N_4/KCC-1 nanocomposite in low pollutant concentrations. The reason for this phenomenon can be increase in by-products and also, decrease the number of activated hydroxyl radicals and positive holes. The regression coefficients (R^2) of kinetic reactions were high values (> 0.93). All of these datasets confirm that the L–H is a suitable model for defining the kinetic of PG degradation under the examined conditions.

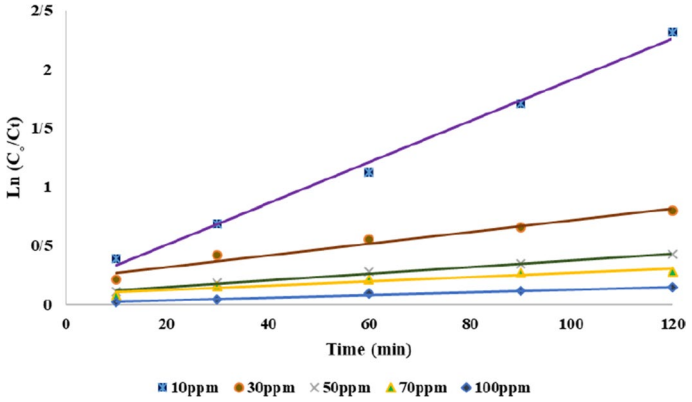

Fig. 15 linear fitting of the kinetic data for PG degradation at different initial concentration

Table 2 Influence of various parameters on the kinetic of PG degradation

Concentration (mg/L)	Kinetic equation, where $Y = \ln\left(\frac{C_0}{C}\right)$ and x = t	k_0 (min^{-1})	$t_{1/2}$ (min)*	R^2
10	y = 0/0175x + 0/1603	17.5×10^{-3}	39.6	0.9943
30	y = 0/005x + 0/2188	5×10^{-3}	138.6	0.9617
50	y = 0/0028x + 0/0961	2.8×10^{-3}	247.5	0.9938
70	y = 0/0018x + 0/861	1.8×10^{-3}	385	0.9357
100	y = 0/0012x + 0/0098	1.2×10^{-3}	577.5	0.9863

*$t_{1/2} = 0.693/k_0$

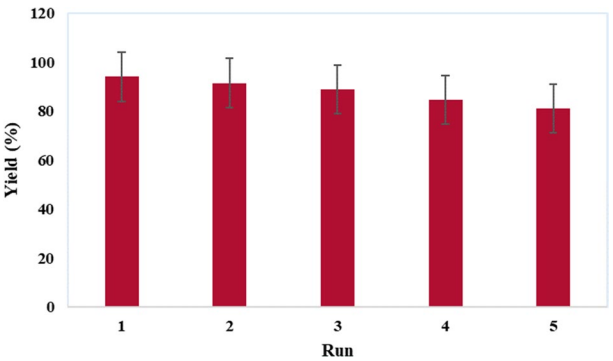

Fig. 16 The reusability of the g-C_3N_4/KCC-1 nanocomposite in photocatalytic degradation of PG under optimum conditions

Reusability and stability of the catalyst

One of the most important factors in photocatalytic processes is the reusability of the catalyst which specifies its stability and activity. For this purpose, the potential

of g-C_3N_4/KCC-1 nanocomposite was measured under optimized conditions in the five cycle reuse. After each experimental run, the catalyst was separated from aqueous dilution using centrifuge and finally washed with water and ethanol. The nanocatalyst shows good stability and there was an insignificant decrease in activity, while (Fig. 16) is proof of this claim. As it is obvious, after five repeated cycles, performance of photocatalytic process decreased from 93.98% to 81.1% eventually. The reason for slight decrease in PG degradation efficiency could be the loss of the catalyst mass during washing and drying processes.

Conclusion

In summary, a novel g-C_3N_4/KCC-1 nanocomposite was prepared via a facile method. Fibrous KCC-1 catalysts are decorated on the g-C_3N_4 nanosheets to the final composite sample exhibit stronger absorption in the light area. For ensuring nanocomposite synthesis, EDAX patterns; FT-IR spectra; XRD patterns; TGA analysis; FE-SEM and TEM images were applied, which proved successful synthesis. The photocatalytic activity of g-C_3N_4/KCC-1 nanocomposite on PG degradation by UV irradiation can be reached up to 93% under optimum condition (pH = 7, nanocomposite dosage = 0.6 g/L, PG concentration = 10 mg/L and contact time = 120 min), and it can be stated that the underlying mechanism of penicillin degradation in this research is oxidation due to positive holes (h+) with top oxidation potential act as producer of hydroxyl radical on g-C3N4/KCC-1 surface from water molecules and generation of radical hydroxyl in neutral solution. Moreover, the result of kinetics shows that the photocatalytic reaction confirmed with the Langmuir–Hinshelwood equation (pseudo-first model) which present an excellent coefficient of regression values. Generally, the results of the present study provide new inspiration for the synthesis of the novel photocatalyst, and extension its practical usage in environmental remediation.

Acknowledgement For the accomplishment of this paper successfully, Birjand University of Medical Sciences (BUMS) has supported us. The authors of this study gratefully acknowledge the Research Council of Birjand University of Medical Sciences (Grant Number: 455815) for the financial support.

References

1. D. Nasuhoglu, A. Rodayan, D. Berk, V. Yargeau, Chem. Eng. J. **189–190**, 41 (2012)
2. A. Almasi, A. Dargahi, M. Mohamadi, H. Biglari, F. Amirian, M. Raei, Electr phys. **8**(9), 2878 (2016)
3. Q. Liang, X. Liu, G. Zeng, Z. Liu, L. Tang, B. Shao et al., Chem. Eng. J. **372**, 429 (2019)
4. J.L. Martinez, Environ. Pollut. **157**(11), 2893 (2009)
5. M. Dehghani, S. Nasseri, M. Ahmadi, M.R. Samaei, A. Anushiravani, J. Environ. Health Sci. Eng. **12**(1), 56 (2014)
6. T.P. Van Boeckel, S. Gandra, A. Ashok, Q. Caudron, B.T. Grenfell, S.A. Levin et al., Lancet Infect Diseases. **14**(8), 742 (2014)
7. J. Zhang, D. Fu, Y. Xu, C. Liu, J. Environ. Sci. **22**(8), 1281 (2010)
8. Gagnon C, Lajeunesse A, Cejka P, Gagné F, Hausler R. Ozone: Science & Engineering; 30(5):387 (2008)

9. K. Kümmerer, Chemosphere **75**(4), 417 (2009)
10. I.A. Alaton, S. Dogruel, E. Baykal, G. Gerone, J. Environ. Manage. **73**(2), 155 (2004)
11. S. Esplugas, D.M. Bila, L.G.T. Krause, M. Dezotti, J. Hazard. Mater. **149**(3), 631 (2007)
12. J. Radjenović, M. Petrović, F. Ventura, D. Barceló, Water Res. **42**(14), 3601 (2008)
13. J. Rivera-Utrilla, G. Prados-Joya, M. Sánchez-Polo, M.A. Ferro-García, I. Bautista-Toledo, J. Hazard. Mater. **170**(1), 298 (2009)
14. Farooq R, Ahmad Z. Physico-Chemical Wastewater Treatment and Resource Recovery: Intech Open. 2017, 109–12 (2017). https://doi.org/10.5772/67803
15. C. Guo, Y. Chen, J. Chen, X. Wang, G. Zhang, J. Wang et al., Bioresour. Technol. **169**, 630 (2014)
16. C. Yang, E.L. Cussler, Biotechnol Bioeng. **69**(1), 66 (2000)
17. M.M. Hossain, J. Dean, Sep. Purif. Technol. **62**(2), 437 (2008)
18. J.W. Peterson, L.J. Petrasky, M.D. Seymour, R.S. Burkhart, A.B. Schuiling, Chemosphere **87**(8), 911 (2012)
19. E.S. Elmolla, M. Chaudhuri, Degradation of the antibiotics amoxicillin, ampicillin and cloxacillin in aqueous solution by the photo-Fenton process. J. Hazard. Mater. **172**(2–3), 1476 (2009)
20. A. Puckowski, K. Mioduszewska, P. Łukaszewicz, M. Borecka, M. Caban, J. Maszkowska et al., J. Pharm Biomed Anal. **127**, 232 (2016)
21. M.S. Saghafinia, S.M. Emadian, M. Vossoughi, Procedia Environ. Sci. **8**, 202 (2011)
22. A. Allahresani, B. Taheri, M.A. Nasseri, Res. Chem. Intermed. **44**(2), 1173 (2017)
23. J. Dai, L. Qin, R. Zhang, A. Xie, Z. Chang, S. Tian et al., Powder Technol. **331**, 162 (2018)
24. Ding Y, Wang X, Fu L, Peng X, Pan C, Mao Q, et al. Science of The Total Environment. 2020:142794 (2020). https://doi.org/10.1016/j.scitotenv.2020.142794
25. D. Wang, F. Jia, H. Wang, F. Chen, Y. Fang, W. Dong et al., J. Coll. Interf Sci. **519**, 273 (2018)
26. P. Wang, T.-T. Lim, Water Res. **46**(6), 1825 (2012)
27. T. Wu, X. Liu, Y. Liu, M. Cheng, Z. Liu, G. Zeng et al., Coord. Chem. Rev. **403**, 213097 (2020)
28. Y. Pan, X. Liu, W. Zhang, Z. Liu, G. Zeng, B. Shao et al., Appl. Catal B: Environ. **265**, 118579 (2020)
29. T. Edvinsson, R. Soc. Open Sci. **5**(9), 180387 (2018)
30. B. Shao, J. Wang, Z. Liu, G. Zeng, L. Tang, Q. Liang et al., J. Mater. Chem. A. **8**(10), 5171 (2020)
31. D. Han, Y. Han, J. Li, X. Liu, K.W.K. Yeung, Y. Zheng et al., Appl. Catal B: Environ. **261**, 118248 (2020)
32. U.G. Akpan, B.H. Hameed, J. Hazard. Mater. **170**(2), 520 (2009)
33. H.R. Pouretedal, M.A. Hasanali, Desalination Water Treat. **51**(13–15), 2617 (2013)
34. A. Fihri, D. Cha, M. Bouhrara, N. Almana, V. Polshettiwar, Chemsuschem **5**(1), 85 (2012)
35. M. Zhang, M. Zhao, R. Chen, J. Liu, Q. Liu, J. Yu et al., Appl. Surf. Sci. **499**, 143933 (2020)
36. F. Zarei, A. Marjani, R. Soltani, Eur. Poly. J. **119**, 400 (2019)
37. F. Shahangi, A.N. Chermahini, M. Saraji, J. Energy chem. **27**(3), 769 (2018)
38. R. Singh, R. Bapat, L. Qin, H. Feng, V. Polshettiwar, ACS Catal. **6**(5), 2770 (2016)
39. M. Ouyang, Y. Wang, J. Zhang, Y. Zhao, S. Wang, X. Ma, TRSC Adv. **6**(16), 12788 (2016)
40. K. Yu, X. Zhang, H. Tong, X. Yan, S. Liu, Mater. Lett. **106**, 151 (2013)
41. S. Cao, J. Low, J. Yu, M. Jaroniec, Adv Mater. **27**(13), 2150 (2015)
42. D.B. Hernández-Uresti, A. Vázquez, D. Sanchez-Martinez, S. Obregón, J. Photochem Photobiol A: Chem. **324**, 47 (2016)
43. A. Aghakhani, E. Kazemi, M. Kazemzad, J. Nanoparticle Res. **17**(10), 386 (2015)
44. A. Khanna, V.K. Shetty, Sol. Energy **99**, 67 (2014)
45. Z. Zhu, Z. Lu, D. Wang, X. Tang, Y. Yan, W. Shi et al., Appl. Catal B: Environ. **182**, 115 (2016)
46. Z. Liu, Y. Jiang, X. Liu, G. Zeng, B. Shao, Y. Liu et al., Comp. Part B: Eng. **173**, 106918 (2019)
47. Y. Li, X. Liu, L. Tan, Z. Cui, X. Yang, Y. Zheng et al., Adv. Funct. Mater. **28**(30), 1800299 (2018)
48. S. Kang, Y. Fang, Y. Huang, L.-F. Cui, Y. Wang, H. Qin et al., Appl Catal B: Environ. **168–169**, 472 (2015)
49. N. Nie, L. Zhang, J. Fu, B. Cheng, J. Yu, Appl. Surf. Sci. **441**, 12 (2018)
50. Y. Li, X. Liu, L. Tan, Z. Cui, D. Jing, X. Yang et al., Adv. Funct. Mater. **29**(20), 1900946 (2019)
51. M. Dhiman, V. Polshettiwar, J. Mater Chem. A. **4**(32), 12416 (2016)
52. N. Bayal, B. Singh, R. Singh, V. Polshettiwar, Sci Rep. **6**, 24888 (2016)
53. C.-H. Weng, Y.-T. Lin, H.-M. Yuan, Sep. Purif. Technol. **117**, 75 (2013)
54. M.A. Lazar, S. Varghese, S.S. Nair, Catalysts. **2**(4), 572 (2012)
55. R. Daghrir, P. Drogui, Environ. Chem. Lett. **11**(3), 209 (2013)
56. J. Li, M. Zhang, Q. Li, J. Yang, Appl. Surf. Sci. **391**, 184 (2017)

57. Z. Tong, D. Yang, T. Xiao, Y. Tian, Z. Jiang, Chem. Eng. J. **260**, 117 (2015)
58. J. Zhang, G. Zhang, X. Chen, S. Lin, L. Möhlmann, G. Dołęga et al., Angewandte Chemie Int. Edition. **51**(13), 3183 (2012)
59. W. Chen, T.-Y. Liu, T. Huang, X.-H. Liu, J.-W. Zhu, G.-R. Duan et al., Appl. Surf. Sci. **355**, 379 (2015)
60. J. Meng, J. Pei, Z. He, S. Wu, Q. Lin, X. Wei et al., RSC Adv. **7**(39), 24097 (2017)
61. A.A. Fauzi, A.A. Jalil, M. Mohamed, S. Triwahyono, N.W.C. Jusoh, A.F.A. Rahman et al., J. Environ. Manage. **227**, 34 (2018)
62. B. Chai, T. Peng, J. Mao, K. Li, L. Zan, Phys. Chem. Chem. Phys. **14**(48), 16745 (2012)
63. J. Wen, J. Xie, X. Chen, X. Li, Appl. Surf. Sci. **391**, 72 (2017)
64. K. Li, Z. Huang, X. Zeng, B. Huang, S. Gao, J. Lu, ACS Applied Mater. Interf. **9**(13), 11577 (2017)
65. Y. He, L. Zhang, M. Fan, X. Wang, M.L. Walbridge, Q. Nong et al., Solar Energy Mater. Solar Cells. **137**, 175 (2015)
66. B. Shao, Z. Liu, G. Zeng, H. Wang, Q. Liang, Q. He et al., J. Mater. Chem. A. **8**(16), 7508 (2020)
67. M.S. Akple, J. Low, S. Wageh, A.A. Al-Ghamdi, J. Yu, J. Zhang, Appl. Surf. Sci. **358**, 196 (2015)
68. R. Hasan, C.C. Chong, S.N. Bukhari, R. Jusoh, H.D. Setiabudi, J. Ind. Eng. Chem. **75**, 262 (2019)
69. Kodal M, Karakaya N, Alchekh Wis A, Ozkoc G. Carbon-Based Nanofiller and Their Rubber Nanocomposites: Elsevier; 2019. p. 325
70. Z. Han, N. Wang, H. Fan, S. Ai, Solid State Sci. **65**, 110 (2017)
71. W. Yu, D. Xu, T. Peng, J. Mater. Chem. A. **3**(39), 19936 (2015)
72. Z. Mohammadbagheri, C.A. Najafi, J. Ind. Eng. Chem. **62**, 401 (2018)
73. X. Xie, C. Mao, X. Liu, L. Tan, Z. Cui, X. Yang et al., ACS Cent. Sci. **4**(6), 724 (2018)
74. . Hitam C, Jalil A, Raji Y. Topics in Catalysis.:1 (2020)
75. B. Zhu, P. Xia, Y. Li, W. Ho, J. Yu, Appl. Surf. Sci. **391**, 175 (2017)
76. M. Hamid, M. Firmansyah, S. Triwahyono, A.A. Jalil, R. Mukti, E. Febriyanti et al., Appl. Catal A: Gen. **532**, 86 (2017)
77. J. Shen, Y. Li, H. Zhao, K. Pan, X. Li, Y. Qu et al., Nano Res. **12**(8), 1931 (2019)
78. S. Xiao, M. Cheng, H. Zhong, Z. Liu, Y. Liu, X. Yang et al., Chem. Eng. J. **384**, 123265 (2020)
79. G. Prados-Joya, M. Sánchez-Polo, J. Rivera-Utrilla, M. Ferro-garcía, Water Res. **45**(1), 393 (2011)
80. P.R. Shukla, S. Wang, H.M. Ang, M.O. Tadé, Sep Purif. Technol. **70**(3), 338 (2010)
81. S. Ahmed, M.G. Rasul, R. Brown, M.A. Hashib, J. Environ. Manage. **92**(3), 311 (2011)
82. V. Homem, L. Santos, J. Environ. Manage. **92**(10), 2304 (2011)
83. X. Zhu, C. Yuan, Y. Bao, J. Yang, Y. Wu, Photocatalytic degradation of pesticide pyridaben on TiO2 particles. J. Mole. Catal A: Chem. **229**(1), 95 (2005)
84. E.S. Elmolla, M. Chaudhuri, Desalination **252**(1), 46 (2010)
85. M.H. Sayadi, S. Sobhani, H. Shekari, J. Clean Prod. **232**, 127 (2019)